this table it may be concluded that the loss of correlation of the quadrupole interaction responsible for deuterium relaxation in a COOD group is dominantly caused by the rotational motions. Thus the slow-exchange limit with respect to the molecular motions may indeed be assumed to be valid approximately. Still, the deuterium exchange should probably be taken into account by at least a correction on the obtained $\tau_\perp$.

Acknowledgment. This work has been carried out under the auspices of The Netherlands Foundation for Chemical Research (SON) with financial aid from the Netherlands Organization for the Advancement of Pure Science (ZWO).

Registry No. Poly(acrylic acid) (homopolymer), 9003-01-4; poly(methacrylic acid) (homopolymer), 25087-26-7.

References and Notes

(1) Lankhorst, D.; Schriever, J.; Leyte, J. C. *Chem. Phys.* **1983**, *77*, 319.
(2) Schriever, J.; Leyte, J. C. *Chem. Phys.* **1977**, *21*, 265.
(3) Halle, B.; Piculell, L. *J. Chem. Soc., Faraday Trans.* **1982**, *78*, 255.
(4) Weiss, S.; Diebler, H.; Michaeli, I. *J. Phys. Chem.* **1971**, *75*, 267.
(5) Selier, P. Thesis, University of Leiden, 1965; Duiser, J. A. Thesis, University of Leiden, 1965.
(6) Craig, L. C.; King, T. P. *J. Am. Chem. Soc.* **1955**, *77*, 6620.
(7) Illingworth, J. A. *Biochem. J.* **1981**, *195*, 259.
(8) Cohn, E. J.; Heyroth, F. F.; Menkin, M. F. *J. Am. Chem. Soc.* **1928**, *50*, 696.
(9) Luz, Z.; Meiboom, S. *J. Chem. Phys.* **1963**, *39*, 366.
(10) Lankhorst, D.; Schriever, J.; Leyte, J. C. *J. Magn. Reson.* **1983**, *51*, 430.
(11) Lankhorst, D.; Schriever, J.; Leyte, J. C. *Ber. Bunsenges. Phys. Chem.* **1982**, *86*, 215.
(12) Hahn, E. L.; Maxwell, E. *Phys. Rev.* **1952**, *88*, 1070.
(13) McConnell, H. M. *J. Chem. Phys.* **1958**, *28*, 430.
(14) Schriever, J.; Westra, S. W. T.; Leyte, J. C. *Ber. Bunsenges. Phys. Chem.* **1977**, *81*, 287.
(15) Costantino, L.; Crescenzi, V.; Quadrifoglio, F.; Vitagliano, V. *J. Polym. Sci., Part A2* **1967**, *5*, 771.
(16) Okubo, T.; Nishizaki, Y.; Ise, N. *J. Phys. Chem.* **1965**, *69*, 3690.
(17) Luz, Z.; Meiboom, S. *J. Am. Chem. Soc.* **1964**, *86*, 4766.
(18) Harned, H. S.; Robinson, R. A. *Trans. Faraday Soc.* **1940**, *36*, 973.
(19) (a) Meiboom, S. *J. Chem. Phys.* **1961**, *34*, 375. (b) Loewenstein, A.; Szöke, A. *J. Am. Chem. Soc.* **1962**, *84*, 1151. (c) Glick, R. E.; Tewari, K. C. *J. Chem. Phys.* **1966**, *44*, 546. (d) Rabideau, S. W.; Hecht, H. G. *Ibid.* **1967**, *47*, 544. (e) Turner, D. L. *Mol. Phys.* **1980**, *40*, 949. (f) Halle, B. Thesis, University of Lund, Sweden, 1981, Chapter 6.
(20) Oosawa, F. "Polyelectrolytes"; Marcel Dekker: New York, 1971; p 88.
(21) Harned, H. S.; Owen, B. B. "The Physical Chemistry of Electrolyte Solutions"; Reinhold Publishing Co.: New York, 1958; p 488.
(22) Luz, Z.; Meiboom, S. *J. Am. Chem. Soc.* **1963**, *85*, 3923.
(23) Klink, J. J. van der; Schriever, J.; Leyte, J. C. *Ber. Bunsenges. Phys. Chem.* **1974**, *78*, 369.
(24) Schriever, J.; Zuiderweg, L. H.; Leyte, J. C. *Mol. Phys.* **1977**, *34*, 635.

Molecular and Crystal Structure of Dextrans: A Combined Electron and X-ray Diffraction Study. 1. The Anhydrous High-Temperature Polymorph†

C. Guizard and H. Chanzy*

Centre de Recherches sur les Macromolécules Végétales‡ (CNRS), 53 X, 38041 Grenoble Cedex, France

Anatole Sarko*

Department of Chemistry, State University of New York, College of Environmental Science and Forestry, Syracuse, New York 13210. *Received April 22, 1983*

ABSTRACT: The crystal and molecular structure of an anhydrous polymorph of a linear, synthetic dextran has been determined through a combined electron and X-ray diffraction analysis and stereochemical model refinement. Electron diffraction data corrected for beam damage were obtained from lamellar single crystals grown from dilute solution and included *hk*0 data to a resolution of 1.1 Å, as well as selected higher layer reflections. The X-ray data in the form of powder patterns were recorded from collections of the same crystals. The structure crystallizes in a monoclinic unit cell with parameters a = 9.22 Å, b = 9.22 Å, c (chain axis) = 7.78 Å, and β = 91.3°. The space group is $P2_1$ with the b axis unique. Two antiparallel-packed molecular chains pass through the unit cell, and the asymmetric unit contains two glucopyranose residues. The base plane of the unit cell is not at right angles to the chain axes. The conformation of the molecule is relatively extended and ribbon-like, with successive glucopyranose residues in a near-twofold screw relationship. The chain conformation is stabilized by one intramolecular hydrogen bond per glucose residue. The chains of like polarity pack into sheets with extensive intrasheet hydrogen bonding. The sheets, packed antiparallel, are likewise extensively bonded together by intersheet hydrogen bonds. The conformational angles ϕ, ψ, and ω show the ϕ angle to be governed by the exo-anomeric effect and the O(6) rotation to be gt. Although the structure resides in a stereochemical energy minimum, the actual conformation could not be predicted by energy minimization methods. The structure solution was straightforward using combined electron diffraction and powder X-ray data, with final residuals R''(electron diffraction) = 0.189 and R(X-ray) = 0.101.

Introduction

During the past 15 years, the crystal structures of many naturally occurring α- and β-(1–3)- and -(1–4)-linked polysaccharides have been determined.[1-7] Both homopolymers and heteropolymers—either in linkage or in sugar residue—are included in this list.[5-7] Many polymorphs, hydrates, and complexes have been characterized, and as a result, a considerable body of information now exists on the structure of these classes of polysaccharides. In the course of these studies, sophisticated procedures for polymer crystal structure refinement have been developed, dealing both with the interpretation of fiber X-ray diffraction data and with stereochemical model analysis.[8]

† Part 15 of the series "Packing Analysis of Carbohydrates and Polysaccharides".
‡ Associé à l'Université Scientifique et Médicale de Grenoble.

0024-9297/84/2217-0100$01.50/0 © 1984 American Chemical Society

Both the successful rate and the degree of precision of the analyses have increased as a result of these computer-based methods. But problems remain, arising mainly from the limited amount of X-ray intensity data available from polycrystalline fiber specimens.

Conspicuous by their absence among the solved structures are the classes of (1–6)-linked polysaccharides. Both the α- and β-(1–6)-glucans (and other glycans) represent large and important groups of naturally occurring polysaccharides. But despite long standing attempts to obtain crystalline fibers of such α- and β-(1–6)-linked homopolysaccharides as dextran and pustulan suitable for X-ray diffraction analysis, there has been no success despite the fact that both structures crystallize in unoriented form.

While crystalline fibers of polysaccharides are sometimes difficult or impossible to obtain, micron-sized single crystals of these substances can be easily grown from dilute solutions, provided low molecular weight fractions are used. The crystals are typical "polymer single crystals" with a platelet morphology.[9] As a rule, the polymer chain axes are perpendicular (or nearly so) to the platelet face. In many cases, these crystals give detailed and well-resolved electron diffraction diagrams. However, electron diffraction data have been used infrequently in polysaccharide structure analysis, usually for unit cell determination only. The intensities, when used, have not been corrected or optimized.[10–14]

The present study was undertaken for all of the above reasons, but principally, to determine the structure of crystalline dextrans. It had previously been shown that good single crystals of dextran could be grown in dilute solutions at different temperatures.[15,16] Two polymorphs could be obtained, depending on temperature, and both gave well-resolved electron diffraction diagrams that appeared to correspond to the X-ray diffraction diagrams of natural dextran polymorphs.[15–17] Given the wealth of electron diffraction data, another objective of this study was to see how well such data could be used to solve a polymer crystal structure in three dimensions.

Experimental Section

Dextran single crystals were grown and collected as described previously.[15] For electron diffraction work, drops of crystal suspension were allowed to dry on carbon-coated grids. Electron diffraction diagrams of individual crystals were recorded on Ilfoset FT35 film, using a Philips EM400T electron microscope equipped with a rotating sample holder and operating at 120 kV. Photographs of typical single crystals and their diffraction diagrams can be found in ref 15.

The relative intensities of *hk*0 reflections in these diagrams were obtained from straight-line optical density tracings of the films, using a Joyce-Loebl recording microdensitometer. The intensity of each reflection was taken as the area under the peak in the tracing, corrected for background density. The intensities were measured in this fashion for a series of diffraction diagrams recorded from a given crystal at regular time intervals, while maintaining a constant electron dose. The measured intensities were then extrapolated to zero time to correct for beam damage. The square roots of the thus corrected intensities were taken directly as the structure factor amplitudes, $F(hk0)$. A total of 47 $F(hk0)$'s were obtained, corresponding to a resolution range of approximately 1.1–1.5 Å. Of these, 38 reflections possessed significant intensity, while an additional 9 were barely detectable and were assigned a minimum observable intensity. The 38 "observed" $F(hk0)$'s were assigned a weight of 1.0 in the subsequent refinement, and the 9 "unobserved" were assigned a weight of 0.5.

For X-ray diffraction, the crystals were allowed to sediment from the suspension and were collected and dried. X-ray diffraction diagrams of collections of crystals were recorded in an evacuated flat-plate camera (Warhus) equipped with 0.25-mm pinhole collimators at a film-to-sample distance of 5 cm. The

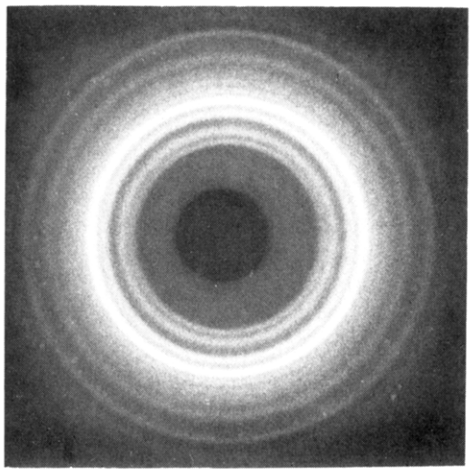

Figure 1. X-ray diffraction diagram of anhydrous dextran (flat film, under vacuum).

diagrams were recorded on Kodak No-Screen film, using Ni-filtered Cu Kα radiation from a Philips X-ray generator operated at 40 kV and 25 mA. A typical exposure time was 20 h. The intensities of the resulting powder diffraction lines were obtained from peak areas of radial density tracings of the films, again using a Joyce-Loebl recording microdensitometer. The intensities of 7 diffraction lines could be measured. The intensities were corrected for the Lorentz and polarization factors appropriate to powder diffraction diagrams. The square roots of the intensities represented the relative structure factor amplitudes, $F(hkl)$. A total of 17 reflections contributed to the 7 measured intensities.

The X-ray diffraction diagram obtained here, shown in Figure 1, may be identical with either diagram L2 or L3 recorded by Jeanes et al. from samples of natural dextran.[17]

The procedures of structure refinement are discussed in appropriate places under Results.

Results

Diffraction Measurements. The unit cell dimensions and the space group had been previously determined from both electron diffraction and X-ray powder pattern measurements on single crystals.[16] The cell was monoclinic with dimensions $a = 9.22$ Å, $b = 9.22$ Å, c (chain axis) = 7.8 ± 0.1 Å, and $\beta = 91.3°$, and the space group was $P2_1$ (b axis unique). The two fold screw axis was, consequently, perpendicular to the chain direction. From the theoretical crystalline density for this unit cell $\rho_{calcd} = 1.63$ g/cm^3, compared with the measured density $\rho_{obsd} = 1.60$ g/cm^3, the above diffraction data indicate two antiparallel-packed chains passing through the unit cell. Each chain contains two anhydroglucopyranose residues within the fiber repeat unit, and there is no water of crystallization in the structure.

Chain Conformation. Because in the (1–6)-linked glucans the linkage between successive anhydroglucopyranose residues contains three bonds (C(5)–C(6)–O-(6)–C(1′)); cf. Figure 2), the length of the residue (the "virtual bond") can be variable, depending on the rotation of atom O(6) about the C(5)–C(6) bond. This necessitated the starting of the structure refinement from various initial monomer models, all differing in the rotational position of the O(6). A minimum of three initial models had to be considered, with the O(6), respectively, in the gt, gg, or tg position. (For a description of this nomenclature, see ref 18). These O(6) rotations correspond to minimum-energy positions found in the crystal structures of mono-, oligo-, and polysaccharides. In practice, however, for each of the above three O(6) positions, at least two rotational positions of the entire monomer residue are possible in the dextran chain. These positions are determined by rotating the residue about the virtual bond while keeping the C(5)–C(6)

Table I
Characteristics of Probable Dextran Conformations Based on Single-Chain Refinement

model	angle, deg ω	ϕ	ψ	τ	VB, Å	conform energy[a]	hydrogen bonds, Å	short contacts
GT1	−69.1	−41.1	173.9	117.5	4.47	14.0		
GT2	−94.9	40.2	118.1	119.9	4.32	18.4		1
GT3	−53.3	−65.1	83.4	111.8	4.47	19.4		
GT4	−58.5	−42.0	61.5	110.9	4.49	21.1		1
GG1	−161.9	−9.7	−108.8	117.9	4.92	15.4		1
GG2	177.9	105.1	140.7	116.7	5.07	35.2		4
TG1	39.2	−11.6	−47.7	118.4	5.00	18.3	O(5)---O(4), 3.02	
TG2	51.7	−169.1	159.2	113.8	5.32	32.2		5

[a] Energy = $\Sigma w_{ij}(d_{ij} - d_{0ij})^2$ in arbitrary units (d_{ij} is the distance in Å between nonbonded atoms i and j, and d_{0ij} is the corresponding equilibrium distance; w_{ij} = weight).

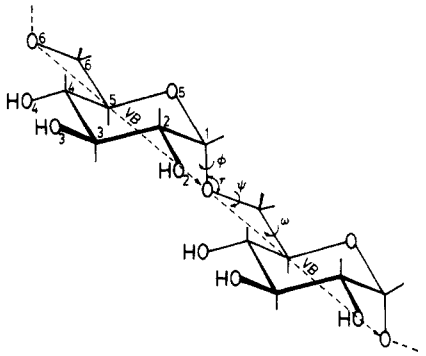

Figure 2. Atom numbering and the definition of bridge angle τ, the glycosidic linkage torsion angles, and the virtual bond (VB). (φ: $H(1)_1$–$C(1)_1$–$O(6)_2$–$C(6)_2$; $\varphi(O)5)$): $O(5)_1$–$C(1)_1$–$O(6)_2$–$C(6)_2$; ψ: $C(1)_1$–$O(6)_2$–$C(6)_2$–$C(5)_2$; ω: O(6)–C(6)–C(5)–H(5)).

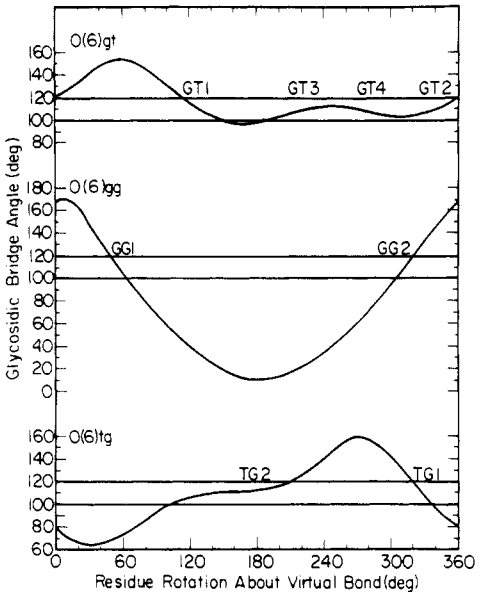

Figure 3. Glycosidic bond angle τ as a function of residue rotation about the virtual bond: top, O(6)gt; middle, O(6)gg; bottom, O(6)tg. The locations of probable models (cf, Table 1) are indicated. Horizontal lines limit the range of probable bridge angles.

rotation fixed at the desired angle. The primary criterion that governs the probability of any of the rotations about the virtual bond is the glycosidic bond angle (the "bridge angle"): it should be within the acceptable range for polysaccharide structures, or, roughly, from 105 to 120°.

As shown in Figure 3, for the three O(6) rotational positions, rotation about the virtual bond produces seven regions of probable chain models with acceptable bridge angles: three for O(6)gt, two for O(6)gg, and two for O(6)tg. Consequently, the structure refinement of dextran was started from these seven regions. The refinement was carried out by using the PS79 program and employing essentially the same strategies as previously described.[8] The initial step in the refinement was to construct the most probable chain conformation(s), as determined by acceptable stereochemistry for an isolated chain.[8] In this refinement, all bond and torsion angles, including rotations about the C(5)–C(6) bond and the virtual bond, were considered variable. The starting atomic coordinate set was the Arnott–Scott average glucose residue.[19]

As shown in Table I, eight acceptable chain models resulted, falling into the seven regions indicated in Figure 3. Most models were essentially free of unacceptable conformational short contacts, although models GG2 and TG2 each had more than one short contact. All models also exhibited a reasonable bridge angle. Only one of the models (TG1) appeared to allow the formation of a rather long, intramolecular hydrogen bond. It also became clear that a single, most probable chain conformation for the dextran structure could not be determined based on the chain stereochemistry alone, as had been possible in other glucans with (1–4)- and (1–3)-glycosidic linkages.

Structure Refinement Although the next step in a typical structure analysis would have been the determination of the most probable packing structures using

Table II
Preliminary Refinement of All Chain Models against Electron Diffraction $F(hk0)$'s

model	R''[a]
GT1	0.573
GT2	0.640
GT3	0.279
GT4	0.628
GG1	0.602
GG2	0.643
TG1	0.645
TG2	0.669

[a] $R'' = \{[\Sigma w(|F_o| - |F_c|)^2]/[\Sigma w|F_o|^2]\}^{1/2}$.

stereochemical refinement, the packing refinement was bypassed here. Instead, it was decided to proceed directly into refinement with electron diffraction (ED) data because the chances of identifying the correct structure using two-dimensional refinement with the relatively large number of $F(hk0)$'s available were thought to be good. This strategy turned out to be correct as only one model produced a sufficiently low residual R'' (cf. Table II for definition of R'') to warrant further refinement. The refinement in this step was carried out with the innermost 20 reflections and only 3 variables: the positioning of the chain axis in the A–B plane of the unit cell, the setting

Table III
Comparison of Structural Features of GT3 Model after Separate (Preliminary) ED and Packing Refinements

structural feature	ED	packing
chain setting angle,[a] deg	34.1	38.6
chain x position, Å	3.05	3.51
chain z position, Å		-1.98
bridge angle τ, deg	113.1	112.5
ϕ, deg	-60.9	-63.1
ψ, deg	77.4	80.3
ω, deg	-53.2	-53.3
packing energy,[b] arb units	18.6	18.7

[a] Rotational position of $O(6)_1$ about chain axis, relative to $-y$ axis. [b] See footnote a in Table I.

angle of the chain (i.e., its rotation about the chain axis), and the rotation of the residue about the virtual bond. For simplicity, a molecular two fold screw axis (i.e., in the chain direction) was assumed to be present, although not required by the space group. The asymmetric unit was thus only one anhydroglucopyranose residue. (The atomic scattering factors used in trhis refinement were the appropriate electron scattering factors.[20])

The results, shown in Table II, clearly pointed to GT3 as the only acceptable model.

As a further check, one cycle of packing refinement was carried out with the GT3 model using the same three variables as in the ED refinement, plus the z translation of the chain. The same stereochemical criteria were used as in the conformation refinement, although the major component in packing energy was now supplied by intermolecular contacts. This refinement was run for two reasons: (1) to check whether the model indicated by ED refinement was close to a stereochemical minimum-energy position, as it should be for the correct structure, and (2) to find the position of the chain along the c axis of the unit cell. As shown in Table III, the structural models obtained both in ED and in packing refinements were virtually identical.

The further refinement of the GT3 model now proceeded in two steps: (1) full refinement of all conformational and packing parameters of the chain (i.e., all torsion and bond angles, and all chain positioning parameters except z translation) against all ED $F(hk0)$'s, followed by (2) the refinement of the z position of the chain against the X-ray $F(hkl)$'s, keeping all other parameters fixed. In the final cycles of these refinements, the constraint of the molecular two fold screw axis in the chain direction was removed, thus basing the structure on a dimer asymmetric unit, in agreement with the requirements of the space group. In addition, in the very fast refinement cycles, the quantity minimized was the function $\Phi = fR'' + (1-f)Y$, which is a linear combination of the residual R'' (denoted in percent) and Y, the sum of all stereochemical energies (i.e., both inter- and intramolecular components), with f a fractional weight to equalize the contributions of both terms in the sum. This ensured against the potential development of unacceptable stereochemical molecular or packing features, which is always a danger in polymer structure refinement with a relatively small number of structure factor amplitudes. An isotropic temperature factor B was also included in these refinements (in the expression $\exp[-B(\sin^2\theta)/\lambda^2]$). Finally, the value of the c axis of the unit cell was also refined within the experimental limits of 7.7 and 7.9 Å, in order to determine its most probable value. The ED and X-ray refinements were alternated until no further improvements in the structure could be gained. The final values for the ED residuals were $R'' = 0.189$ and $R = 0.180$.

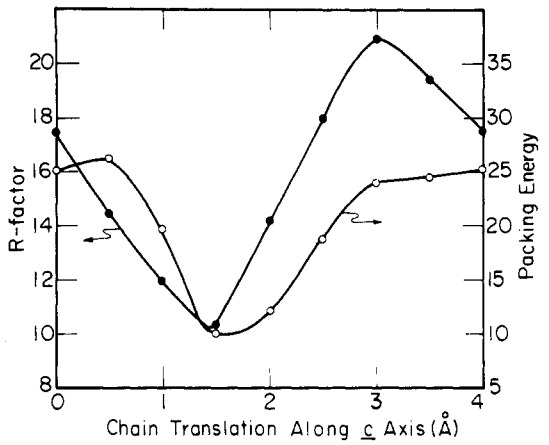

Figure 4. X-ray R factor and total packing energy (Y) as a function of the position of the chain along the c unit cell axis.

Table IV
Summary of the Main Structural Features of the Final Dextran Structure[a]

feature (indiv residues)	final structure	packing pred
unit cell c, Å	7.78	7.78[b]
n	2[b]	2[b]
h_1, h_2, Å	3.91, 3.87	3.90, 3.88
VB_1, VB_2, Å	4.47, 4.44	4.46, 4.44
ω_1, ω_2,[c] deg	-53.8, -50.6	-53.3, -51.7
ϕ_1, ϕ_2,[c] deg	-55.5, -56.2	-56.0, -55.8
$\phi(0(5))_1$, $\phi(0(5))_2$,[c] deg	62.9, 64.5	64.3, 63.8
ψ_1, ψ_2,[c] deg	67.9, 68.0	68.8, 68.2
τ_1, τ_2,[c] deg	116.6, 115.4	116.6, 114.6
position of chain in unit cell: x, y, z (Å)	3.549, 0, 1.241	3.525, 0, 1.345
chain setting angle, deg	24.9	25.2
intermolecular energy	14.7	12.4
intramolecular energy	34.5 total; 17.3 per residue	36.3 total; 18.2 per residue
short contacts	none	none
hydrogen bonds	6 intermolecular, 2 intramolecular	6 intermolecular, 2 intramolecular
ED residuals: R,R'' (isotropic B)[d]	0.180, 0.189 (0)	
X-ray residuals: R,R'' (isotropic B)[d]	0.101, 0.116 (0)	

[a] The features of the best predicted packing structure are shown for comparison. [b] Constrained by diffraction data. [c] See Figure 2. [d] $R = \Sigma||F_o| - |F_c||/\Sigma|F_o|$.

The z-translation refinement against the X-ray data quickly resulted in a minimum in the X-ray residual $R = 0.101$ at $z = 1.241$ Å. Because the number of observed X-ray $F(hkl)$'s was small, a check was made to see that only one R minimum was present and that it coincided with the packing energy minimum. This was done simply by calculating both R and the packing energy at 0.5-Å intervals for chain translation along the z axis. As shown in Figure 4, only one minimum was present for both values, at coinciding z axis positions.

Similarly, a relatively broad minimum in ED, X-ray, and stereochemical refinements occurred for the c parameter in the range 7.76–7.80 Å. The best structure was, consequently, taken to have $c = 7.78$ Å, at the midpoint of the range.

The main characteristics of the final structure are given in Table IV, its hydrogen bonds are shown in Table V, and

Table V
Hydrogen Bond Distances and Angles

hydrogen bond[a]	O---O length, Å	angle,[b] deg
Intramolecular		
$O(4)_1$---$O(2)^{i}_1$	2.997	128
$O(4)_2$---$O(2)^{i}_2$	2.981	129
Intermolecular		
$O(2)_2$---$O(3)^{ii}_1$	3.119	78
$O(3)_1$---$O(4)^{iv}_2$	2.638	105
$O(2)_2^{v}$---$O(3)_1$	2.852	139
$O(4)_2^{iv}$---$O(4)_1$	2.873	96
$O(2)_1$---$O(3)^{iii}_2$	2.944	100
$O(3)_2^{vi}$---$O(5)_2$	2.903	128
$O(2)_1$---$O(6)^{iv}_1$ (?)	2.860	112

[a] Atom subscripts indicate residue number; superscripts i–vi indicate symmetry-related atoms as follows: (i) $x, y, z + 1$; (ii) $x - 1, y, z + 1$; (iii) $x + 1, y, z$; (iv) $1 - x, y + {}^1/_2, 1 - z$; (v) $1 - x, y + {}^1/_2, 2 - z$; (vi) $-x, y + {}^1/_2, 2 - z$. [b] The hydrogen bond angle is the angle θ at the donor oxygen:  An angle of approximately 110° corresponds to a linear hydrogen bond.

Table VI
Cartesian Coordinates of Final Structure (Å)

atom	x	y	z
$C(1)_1$	4.845	−0.138	4.927
$C(2)_1$	6.330	0.226	5.027
$C(3)_1$	6.788	1.082	3.848
$C(4)_1$	6.401	0.453	2.518
$C(5)_1$	4.915	0.074	2.540
$C(6)_1$	4.508	−0.718	1.300
$O(2)_1$	6.611	0.824	6.294
$O(3)_1$	8.203	1.216	3.868
$O(4)_1$	6.629	1.375	1.460
$O(5)_1$	4.611	−0.749	3.680
$O(6)_1$	3.099	−0.971	1.241
$H(1)_1$	4.634	−0.842	5.676
$H(2)_1$	6.871	−0.673	4.984
$H(3)_1$	6.350	2.033	3.921
$H(4)_1$	6.978	−0.409	2.359
$H(5)_1$	4.340	0.951	2.589
$H(6a)_1$	5.029	−1.630	1.280
$H(6b)_1$	4.780	−0.164	0.450
$C(1)_2$	2.263	0.152	8.818
$C(2)_2$	0.790	−0.261	8.921
$C(3)_2$	0.358	−1.127	7.739
$C(4)_2$	0.726	−0.484	6.411
$C(5)_2$	2.207	−0.083	6.426
$C(6)_2$	2.610	0.732	5.201
$O(2)_2$	0.545	−0.893	10.179
$O(3)_2$	−1.048	−1.339	7.771
$O(4)_2$	0.513	−1.393	5.338
$O(5)_2$	2.478	0.753	7.563
$O(6)_2$	4.017	0.998	5.150
$H(1)_2$	2.465	0.860	9.567
$H(2)_2$	0.215	0.617	8.893
$H(3)_2$	0.841	−2.057	7.808
$H(4)_2$	0.135	0.372	6.264
$H(5)_2$	2.601	−0.980	6.802
$H(6a)_2$	2.082	1.639	5.194
$H(6b)_2$	2.345	0.190	4.342

the atomic coordinates are listed in Table VI. The comparisons of calculated and observed structure factor amplitudes—for both ED and X-ray data—are given in Table VII. A stereoview of a chain section and a unit cell projection are shown in Figure 5.

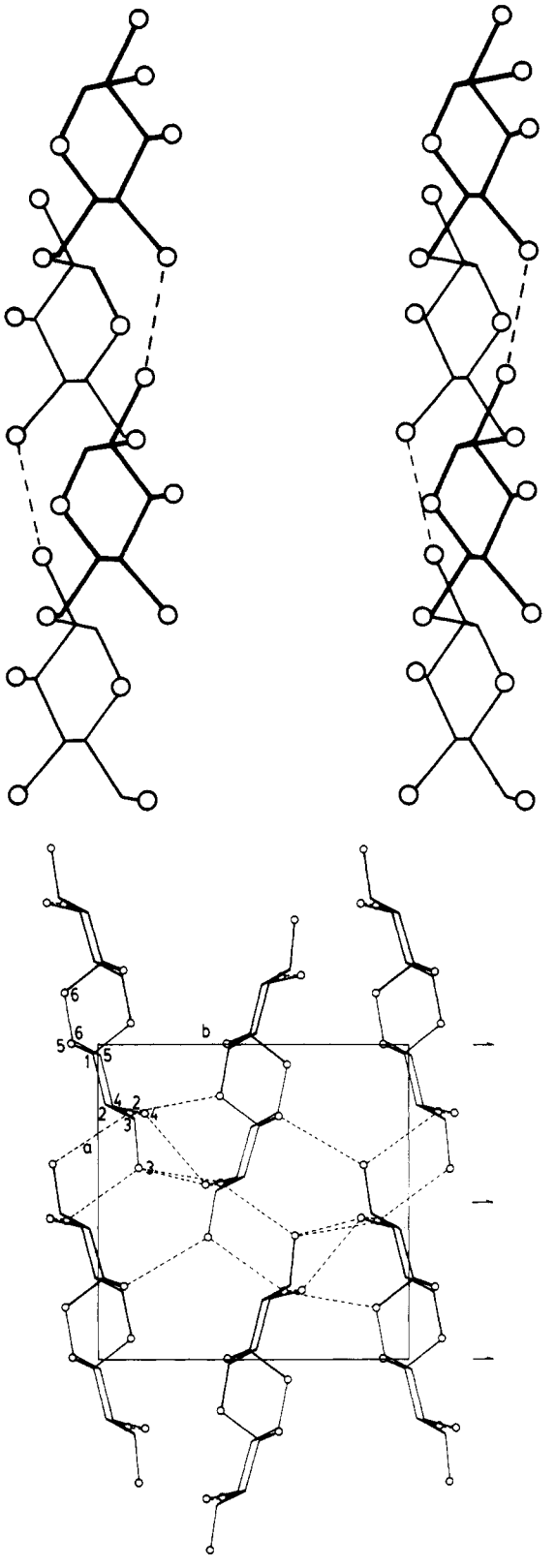

Figure 5. Top: Stereoview of chain seen from the *a* direction of the unit cell. Bottom: Projection of unit cell down the *c* axis. Hydrogen bonds are indicated by dashed lines; hydrogen atoms are not shown. Corner chain has "up" polarity; center chain is "down".

Discussion

Structural Characteristics. Several features of this dextran polymorph are noteworthy. First, the crystal structure contains no water, even though dextran is an easily water-soluble polysaccharide. (This may be a consequence of the fact that the crystals were grown under pressure at temperatures between 120 and 200 °C. With crystallization conditions below 100 °C, another crystalline dextran polymorph is obtained which is a hydrate). The chain conformation is relatively extended, with the chain

Table VII
Comparison of Calculated and Observed Structure Factor Amplitudes

A. Electron Diffraction

hkl	F_c	F_o	*hkl*	F_c	F_o
100	6.2	6.9[a]	520	6.7	8.3
110	12.8	11.1	250	5.0	7.0
200	2.0	4.9[a]	440	1.0	3.4
020	42.4	34.8	530	0.4	3.0
210	10.9	11.6	350	5.8	5.1
120	14.4	14.4	600	5.3	5.4
220	25.3	22.0	060	2.3	4.0
300	4.1	5.0	610	7.2	7.3
310	5.0	7.5	160	3.1	2.2[a]
130	9.0	10.5	620	4.1	4.3
320	4.7	4.7	260	0.8	2.2[a]
230	9.0	10.1	540	3.2	2.5
400	17.4	16.1	450	0.9	2.2[a]
040	10.7	9.4	630	2.2	3.2
410	11.4	11.5	360	4.5	2.2[a]
140	4.3	6.1	550	3.0	2.2[a]
330	6.3	5.0	170	2.1	2.2[a]
420	11.1	12.2	640	2.1	2.2[a]
240	8.2	9.8	720	8.6	6.3
500	18.8	15.6	730	7.0	6.6
430	8.8	9.2	650	1.6	2.2[a]
340	6.4	4.9	740	5.3	4.7
510	6.9	6.6	750	5.0	4.3
150	1.6	2.2[a]			

B. X-ray Diffraction

hkl	$F(hkl)$	$F_{calc} = [\Sigma F(hkl)^2]^{1/2}$	F_o
110	73.6	73.6	68.7
020	156.4		
200	4.7	156.5	176.5
120	95.8		
$2\bar{1}0$	46.4	106.5	118.0
$\bar{1}01$	47.2		
101	64.0		
011	30.7	85.3	62.6
$1\bar{1}1$	99.6		
$\bar{1}11$	87.1	132.3	120.8
021	66.3		
$2\bar{0}1$	44.2		
$\bar{2}01$	37.1	87.9	95.7
$\bar{1}21$	105.7		
121	28.6		
$2\bar{1}1$	44.3		
$\bar{2}11$	58.6	131.9	131.9

[a] Unobserved reflection.

parameters $n = 2$, $h(\text{av}) = 3.89$ Å and residue length VB(av) = 4.46 Å. The glycosidic bridge angle $\tau(\text{av}) = 116.0°$, which is only slightly outside the 110.9–115.5° range of bridge angles for the seven oligosaccharides with the α-(1–6) linkage whose crystals structures have been determined.[21] The rotational position of the O(6) relative to the pyranose ring $\omega(\text{av}) = -52.2°$, or less than 8° from the exact gt position (−60°). The angle $\varphi(\text{O}(5))(\text{av}) = 63.7°$, which is less than 4° from the 60° position expected for this angle on the basis of the exo-anomeric effect operating in anhydroglucopyranose structures.[22] The chain conformation, although based on a dimer asymmetric unit as dictated by the space group symmetry, is virtually indistinguishable from a conformation in which a two fold screw axis coincides with the chain axis. The conformation is stabilized by one, rather long, intramolecular hydrogen bond per residue: $\text{O}(2)_{1,2}\cdots\text{O}(4)_{3,4}(\text{av}) = 2.99$ Å.

Several attempts have been previously made to predict the conformation of the dextran chain. The first of these attempts was by Rees and Scott, who, on the basis of hard-sphere calculations, concluded that the dextran chain should be "very flexible but, on the average, rather extended".[23] Although, qualitatively, this prediction was correct, quantitatively their estimates of the probable values for the chain parameters n and h were in the form of wide ranges, with $n = 2$–7 and $h = 6$ to +6 Å. They did not attempt to predict the value of the angle ω.

More recently, the same type of prediction was attempted by Tvaroska et al., using a conformational calculation based on pairwise potential energy functions complete with hydrogen-bond and torsional energy terms.[21] The ranges of n and h could not be narrowed, but two probable values of ω were found, those corresponding to gt and gg positions. The latter was judged to be slightly more probable of the two, and a total of six conformations, all differing in φ and ψ angles but with little differences in their energies, were predicted.[21] Comparing now the actual φ, ψ, and ω values (cf. Table IV) with those predicted by Tvaroska et al.,[21] one can see that the real structure is not near any of the predicted energy minima, although it does reside within the theoretically allowed conformational space.

Our own predictions of the most probable chain conformation were not much better, even with the help of n and h values fixed by diffraction measurements. As shown in Table I and Figure 3, the actual model—even though it is among the predicted models—has a conformational energy that is higher than that of four other models and considerably higher than the predicted lowest energy conformation. (The latter, incidentally, coincides with one of the minimum-energy structures of Tvaroska et al.,[21] although not with their global minimum).

The lack of agreement between all of these predictions and the actual structure serves as a reminder that our predictive methods are still much less reliable with flexible structures than they are with the stiffer (1–4)- and (1–3)-linked polysaccharides. The oligosaccharide crystal structures were, likewise, not of much help, because none of the seven known structures possesses the same combination of φ, ψ, and ω angles as occurs in dextran.[21] In fact, only one of the seven structures (planteose) has the same ω angle and none has the same ψ angle. The φ angles are more consistent: all seven structures have φ angles falling in the range −36 to −61°. Most likely, this relatively narrow range is a consequence of the exo-anomeric effect.[22] It would be very useful to determine the crystal structures of a series of isomaltodextrins, in order to learn more about the α-(1–6) linkage in this homologous series.

The conformation flexibility of the dextran chain is probably the underlying reason that dextran does not crystallize as an oriented fiber. Apparently, attempts to extend and orient the chains by drawing tend to place chain segments in a variety of conformational minima, rather than into a single one, thus preventing crystallization. Relaxation of the tension followed by sufficient heating of the fiber to give chain segments mobility, but not melt the fiber, results in crystallization but loss of orientation.

The packing of the dextran chains in the crystal lattice also shows some interesting features. One is that the unit cell is monoclinic with the angle $\beta \neq 90°$; i.e., the a–b plane of the cell is not at right angles to the chain axis. Dextran appears to be the first of the polysaccharides studied thus far to possess such a cell. Because the β angle, at 91.3°, is very little different from 90°, it is doubtful that its value would have been correctly determined from a fiber X-ray diagram, had the latter been available. One wonders if there are other structures of polysaccharides with similar monoclinic unit cells whose structures have not been

correctly determined in all details by X-ray diffraction.

The crystalline packing of dextran is quite dense (ρ_{calcd} = 1.63 g/cm^3), undoubtedly reflecting the fact that the structure is nearly maximally hydrogen bonded. All of the hydroxyl oxygens participate in at least two hydrogen bonds each, one of the O(5) atoms receives one hydrogen bond, and the only oxygen atom not hydrogen bonded is the other O(5). Both inter- and intramolecular hydrogen bonds are present, forming three sequences:

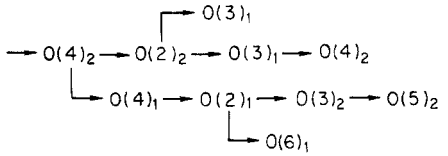

The main sequence is an infinite chain linking together dextran chains of both polarity and containing both inter- and intramolecular bonds; the longer of the two branches links together the remaining oxygen atoms, also inter- and intramolecularly, while the short branch loops back to the infinite sequence. The donor–acceptor sequence drawn above is not based on experimental evidence, but it is the most probable one and is in good agreement with the calculated C–OH→O angles, shown in Table V. Two of the hydroxyls ($O(2)_2$ and $O(4)_2$) form a bifurcated bond while one of the hydroxyls ($O(3)_1$) accepts two hydrogen bonds. Also, as shown in the above sequence, there is a possible intermolecular hydrogen bond between $O(2)_1$ and $O(6)_1$, with a length of 2.86 Å. Although no hydrogen bonds to the glycosidic oxygen have been observed to date in any of the α- and β-(1–3)- and -(1–4)-linked polysaccharide crystal structures, perhaps in (1–6)-linked structures such hydrogen bonds may be more favorable.

The consequence of these hydrogen-bond sequences is that the chains of the same polarity form sheets along the *a* direction of the unit cell. The hydrogen bonds run both in *a* and *c* directions within the sheets, and the latter are bonded together by several additional hydrogen bonds. Given this nearly maximal hydrogen bonding of the structure, coupled with a fairly extended chain conformation, crystalline dextran can be expected to be insoluble in water. Other, similarly extended and extensively hydrogen-bonded crystalline polysaccharides, notably cellulose II[24] and pseudonigeran (α-(1–3)-D-glucan[4]), are completely water insoluble. In fact, even though amorphous dextran is soluble in water, it becomes insoluble upon crystallization.

Methods. This structure was solved essentially with electron diffraction data. It is probably the first polymer crystal structure in which such reliance on quantitative, optimized ED data has been made. Without the ED data, the structure could not have been solved, and it is also clear that it could not have been correctly predicted.

As shown above, the combined use of the ED and X-ray data, augmented by the stereochemical procedures, has resulted in a great deal of structural detail. In addition, some very useful methodology information has been obtained. Among the structural detail that probably would not have been forthcoming from a comparable fiber X-ray study were the accurate unit cell parameters and a firm determination of the space group. From this information, all other structural detail followed.

From the point of view of methodology, it is clear that with thin, lamellar single crystals, the kinematic scattering approximation is valid and accurate ED intensities can be obtained, provided some precautions and corrections are applied. Among them, the elimination of beam damage by measurement of intensities at various exposure times and their extrapolation to zero time is certainly critical. The knowledge of the crystal mosaic structure and the determination of the fraction of the crystal volume that contributes to each diffraction spot would be another worthwile correction. The latter, however, was not applied here. Whether the use of n-beam dynamic scattering[25,26] and crystal bending[27] corrections may provide additional improvements remains to be determined.

Another important point concerning methodology was the realization that if an accurately controllable electron microscope goniometer stage is available, the third dimension of the unit cell can be determined from the observation of higher level reflections.[16] Even though this information may not be as accurate as the other unit cell parameters, given a sufficiently large number of reflection intensities, the third dimension can be refined to an accurate value, as demonstrated here.

Finally, the combined use of ED and powder X-ray data has clearly demonstrated the utility of this methodology. Fiber X-ray diagrams frequently show severe arcing of reflections, caused by the disorientation of crystallites. Such arcing may cause large uncertainties in the measurement of integrated X-ray reflection intensities. In such cases, it would be better to measure intensities from powder patterns, but the overlapping of lines usually seen in the latter may negate any advantages of more precise intensity measurement. However, when ED data are available—even if not of the best quantitative type—such data can be used to index the powder patterns accurately and help resolve partially overlapped lines into individual intensities. It is probable that under some circumstances, such as where the ED intensities are not entirely reliable but the unit cell parameters are, a structure could be solved only on the basis of powder intensity data. The Rietveld method may be particularly useful in such cases.[28] It would now be of interest to determine how close to the correct structure one could come with the latter method.

Acknowledgment. This work has been supported by NSF Research Grants CHE-7727749 and CHE-8107534 and by NATO Grant No. RG 1386.

Registry No. Dextran, 9004-54-0.

References and Notes

(1) A. Sarko, *Tappi*, **61**, 59 (1978).
(2) A. Sarko and P. Zugenmaier, in *ACS Symp. Ser.* **No. 141**, 459 (1980).
(3) Y. Deslandes, R. H. Marchessault, and A. Sarko, *Macromolecules* **13**, 1466 (1980).
(4) K. Ogawa, K. Okamura, and A. Sarko, *Int. J. Biol. Macromol.*, **3**, 31 (1981).
(5) K. Taylor, Ph.D. Thesis, Université de Montréal, 1976.
(6) S. Arnott and W. T. Winter, *Fed. Proc., Fed. Am. Soc. Exp. Biol.*, **36**, 73 (1977).
(7) K. Okuyma, S. Arnott, R. Moorhouse, M. D. Walkinshaw, E. D. T. Atkins, and C. Wolf-Ullish, in *ACS Symp. Ser.*, **No. 141**, 411 (1980).
(8) P. Zugenmaier and A. Sarko, in *ACS Symp. Ser*, **No. 141**, 225 (1980).
(9) P. H. Geil, "Polymer Single Crystals", Interscience, New York, 1963.
(10) W. Claffey, K. Gardner, J. Blackwell, J. Lando, and P. H. Geil, *Philos. Mag.*, **30**, 1223 (1974).
(11) H. Hasegawa, W. Claffey, and P. H. Geil, *J. Macromol. Sci., Phys.*, **B13**, 89 (1977).
(12) F. Brisse and R. H. Marchessault, in *ACS Symp. Ser.* **No. 141**, 267 (1980).
(13) E. Roche, H. Chanzy, M. Boudeulle, R. H. Marchessault, and P. R. Sundararajan, *Macromolecules*, 11, 86 (1978).
(14) S. Pérez, M. Roux, J. F. Revol, and R. H. Marchessault, *J. Mol. Biol.*, **129**, 113 (1979).
(15) H. Chanzy, C. Guizard, and A. Sarko, *Int. J. Biol. Macromol.*, **2**, 149 (1980).
(16) H. Chanzy, G. Excoffier, and C. Guizard, *Carbohydr. Polym.* 1, 67 (1981).

(17) A. Jeanes, N. C. Schieltz, and C. A. Wilham, *J. Biol. Chem.*, **176**, 617 (1948).
(18) A. Sarko and R. H. Marchessault, *J. Polym. Sci., Part C*, **28**, 317 (1969).
(19) S. Arnott and W. E. Scott, *J. Chem. Soc., Perkin Trans. 2*, 324 (1972).
(20) P. A. Doyle and J. M. Cowley, "International Tables for X-Ray Crystallography", J. A. Ibers and W. C. Hamilton, Eds., Kynoch Press, Birmingham, England, Vol. IV, p 152.
(21) I. Tvaroska, S. Pérez, and R. H. Marchessault, *Carbohydr. Res.*, **61**, 97 (1978).
(22) S. Pérez and R. H. Marchessault, *Carbohydr. Res.*, **65**, 114 (1978).
(23) D. A. Rees and W. E. Scott, *J. Chem. Soc. B*, 469 (1971).
(24) A. J. Stipanovic and A. Sarko, *Macromolecules*, **9**, 851 (1976).
(25) B. Moss and D. L. Dorset, *J. Macromol. Sci., Phys.*, **B22**, 69 (1983).
(26) D. L. Dorset and B. Moss, *Polymer*, **24**, 291 (1983).
(27) B. Moss and D. L. Dorset *J. Polym. Sci., Polym. Phys. Ed.*, **20**, 1789 (1982).
(28) H. M. Rietveld, *J. Appl. Crystallogr.*, **2**, 65 (1969).

Kinetic Studies on Cationic Ring-Opening Polymerization of 2-Phenyl-1,2-oxaphospholane

Shiro Kobayashi, Masato Suzuki, and Takeo Saegusa*

Department of Synthetic Chemistry, Faculty of Engineering, Kyoto University, Kyoto 606, Japan. *Received March 14, 1983*

ABSTRACT: A kinetic study on the cationic ring-opening polymerization of a five-membered deoxophostone (2-phenyl-1,2-oxaphospholane (**1**)) was performed with the use of the four initiators $MeOSO_2CF_3$ (MeOTf), MeI, $PhCH_2Br$, and $PhCH_2Cl$. The course of polymerization was monitored by ^{31}P NMR spectroscopy for kinetic analysis. The rate constants and activation parameters of the propagation were obtained. The nature of the propagating species and the rate constant of propagation varied significantly according to the initiators. The polymerization of **1** with MeOTf proceeded via a cyclic phosphonium propagating species. With alkyl halide initiators, on the other hand, the propagating species were of the covalent alkyl halide type. The magnitude of k_p was in the following order: MeI $\gtrsim$ MeOTf > $PhCH_2Br$ > $PhCH_2Cl$. The present study provides the first example that a covalent-type propagating species of an alkyl iodide showed even larger propagation reactivity than an onium type with a OTf^- counteranion.

Recently, we reported the cationic ring-opening polymerization of a five-membered deoxophostone (2-phenyl-1,2-oxaphospholane (**1**)) to give poly(phosphine oxide) **2**[1] and the reduction of the phosphoryl group of **2** to yield polyphosphine **3**.[2] A new polymer having **2** as a graft chain has been shown to exhibit good chelating properties toward heavy-metal ions.[3]

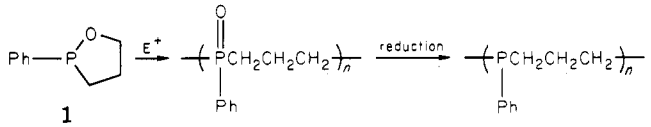

1 2 3

Several cyclic phosphorus(III) compounds (**4**) have been polymerized with a cationic initiator via the Arbuzov-type reaction to give polymers of a phosphinate or phosphonate unit ("normal unit", **5a**).[4-11] During the polymerization,

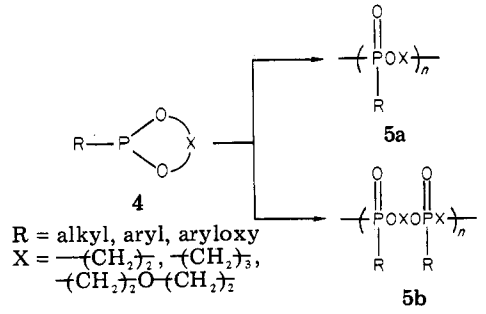

4

R = alkyl, aryl, aryloxy
X = $-(CH_2)_2-$, $-(CH_2)_3-$, $-(CH_2)_2O(CH_2)_2-$

however, a side reaction takes place to form an isomerized unit (**5b**). The amount of the isomerized unit **5b** is dependent on the reaction conditions, and it sometimes exceeds that of a normal unit **5a**.[8,9] Therefore, the kinetics on cationic ring-opening polymerizations of cyclic phosphorus(III) monomers are complicated, and, in fact, the polymerization has not been precisely performed except for the phosphocane polymerization.[11] The cationic ring-opening polymerization of **1** in the present study has been found to be a clean system to yield a polymer consisting exclusively of "normal unit" **2** without isomerization, and hence, is a suitable system for kinetic study.

Results and Discussion

MeOTf-Initiated System. Figure 1a shows the ^{31}P NMR spectrum of the MeOTf-initiated polymerization system that was recorded immediately after the addition of MeOTf to the monomer solution at 0 °C in PhCN. For the purpose of the kinetic analysis, the monomer/initiator molar ratio was adjusted to 10.0. The two peaks (A and B) were assigned as A (+109 ppm relative to external 85% H_3PO_4 standard) for monomer **1** and B (+101 ppm) for the methylated phosphonium ion (**6**). The initiation reaction was so fast that production of the first propagating species of the cyclic phosphonium (**6**) had already finished. The phosphonium species **6** has been identified also by a model experiment in which an equimolar reaction of **1** with MeOTf in PhCN was carried out. The reaction mixture showed the following characteristic NMR signals for three nuclei: ^{31}P NMR (+101 ppm, single peak), ^{19}F NMR (+0.47 ppm relative to external CF_3CO_2H standard, assignable to $CF_3SO_3^-$), and ^1H NMR (a doublet at δ 2.7 due to CH_3P^+, $^2J_{HP}$ = 14.3 Hz, and double triplets at δ 4.9 due to CH_2OP^+, $^3J_{HP}$ = 10.1 Hz and J_{HH} = 6.0 Hz). These data support cyclic structure **6**, which was stable at a higher temperature, e.g., 60 °C.

On heating at 70 °C two new signals appeared (Figure 1b). Signal C (+38 ppm) was ascribed to phosphine oxide unit **2** and signal D (+34 ppm) was assigned as a terminal

0024-9297/84/2217-0107$01.50/0 © 1984 American Chemical Society